

ARTICLE

Received 13 Mar 2015 | Accepted 9 Dec 2015 | Published 21 Jan 2016

DOI: 10.1038/ncomms10418

OPEN

# Engineered Mott ground state in a $\text{LaTiO}_{3+\delta}/\text{LaNiO}_3$ heterostructure

Yanwei Cao<sup>1</sup>, Xiaoran Liu<sup>1</sup>, M. Kareev<sup>1</sup>, D. Choudhury<sup>1,2</sup>, S. Middey<sup>1</sup>, D. Meyers<sup>1</sup>, J.-W. Kim<sup>3</sup>, P.J. Ryan<sup>3</sup>, J.W. Freeland<sup>3</sup> & J. Chakhalian<sup>1</sup>

In pursuit of creating cuprate-like electronic and orbital structures, artificial heterostructures based on  $\text{LaNiO}_3$  have inspired a wealth of exciting experimental and theoretical results. However, to date there is a very limited experimental understanding of the electronic and orbital states emerging from interfacial charge transfer and their connections to the modified band structure at the interface. Towards this goal, we have synthesized a prototypical superlattice composed of a correlated metal  $\text{LaNiO}_3$  and a doped Mott insulator  $\text{LaTiO}_{3+\delta}$ , and investigated its electronic structure by resonant X-ray absorption spectroscopy combined with X-ray photoemission spectroscopy, electrical transport and theory calculations. The heterostructure exhibits interfacial charge transfer from Ti to Ni sites, giving rise to an insulating ground state with orbital polarization and  $e_g$  orbital band splitting. Our findings demonstrate how the control over charge at the interface can be effectively used to create exotic electronic, orbital and spin states.

<sup>1</sup>Department of Physics, University of Arkansas, Fayetteville, Arkansas 72701, USA. <sup>2</sup>Department of Physics, Indian Institute of Technology Kharagpur, Kharagpur 721302, India. <sup>3</sup>Advanced Photon Source, Argonne National Laboratory, Argonne, Illinois 60439, USA. Correspondence and requests for materials should be addressed to Y.C. (email: yc003@uark.edu).

Understanding and controlling the interactions between charge, spin, orbital and structural degrees of freedom in transition-metal oxides is at the centre of modern condensed matter physics<sup>1–3</sup>. In recent years, inspired by the tremendously successful research on physics and applications of ultra-thin semiconductor heterostructures, multilayers of correlated complex oxides have become a platform of choice to generate the emergent electronic and magnetic states, unattainable in the bulk compounds<sup>4–14</sup>. The inherent many-body nature of the correlated states, however, raises many fundamental questions that demand experimental validation and expansibility about the applicability of the concepts and formulas developed for semiconductor heterointerfaces<sup>6</sup>. Recent experimental work on complex oxide interfaces<sup>5–14</sup> revealed a remarkable importance of the electronic configurations of partially filled *d*-shell transition-metal ions for understanding the emerging many-body phenomena<sup>1–3</sup>, including the Ti  $3d^1$  configuration in the SrTiO<sub>3</sub>-based two-dimensional electron gases<sup>5</sup>, Cu  $3d^9\bar{\text{L}}$  configuration in the orbitally and magnetically reconstructed states at the manganate-cuprates interfaces (here  $\bar{\text{L}}$  denotes a ligand hole on the oxygen ion)<sup>6,15</sup> and Ni  $3d^8\bar{\text{L}}$  configuration in self-doped and orbitally polarized nickelate heterojunctions<sup>2,6,16–19</sup>. To induce a specific electronic configuration at the interface, charge transfer (or electron doping) has been proven to be a particularly powerful tool to achieve this goal<sup>20–22</sup>. Even more so than in the doped semiconductors<sup>23–26</sup>, charge transfer with strong electron–electron correlations and frustrated spin and orbital interactions at the interface may give rise to unexpected collective quantum states not attainable with semiconductor heterojunctions<sup>4–6</sup>. Understanding the mechanism of charge redistribution between layers of Mott materials and the implications of a specific electron reconfiguration arising from the charge transfer is therefore of a great necessity towards the rational design of applications based on strongly correlated electrons<sup>6,20–22</sup>.

In semiconductor heterostructures, the charge transfer can be successfully rationalized in terms of single-electron energy states to profile the energy band bending and the band alignments across the interface<sup>26,27</sup>. Following this notion, we recap that within the class of complex oxides with  $3d$  electrons there are two types of Mott insulating behaviour parameterized in the Zaanen–Sawatzky–Allen scheme by the relative magnitude of on-site Coulomb repulsion energy  $U_{\text{dd}}$  between *d*-shell electrons versus charge-transfer energy  $\Delta_{\text{CT}}$  between oxygen *p*-shell and the TM *d*-state<sup>28</sup>; based on this, one can distinguish between Mott–Hubbard insulators (MHI,  $U_{\text{dd}} < \Delta_{\text{CT}}$ ) and charge-transfer insulators or charge-transfer metals (CTM,  $U_{\text{dd}} > \Delta_{\text{CT}}$ )<sup>1,2</sup>. To date, the vast majority of experimental and theoretical work has been focused on charge doping at the interfaces between MHI and MHI<sup>29,30</sup>, and MHI and normal metal<sup>31–34</sup>. Some of the most remarkable physical phenomena such as high- $T_{\text{C}}$  superconductivity and colossal magnetoresistance, however, are observed in charge-transfer compounds characterized by the strong hybridization between oxygen  $2p$  and transition metal  $3d$  states, complex electronic configurations (for example, mixing between  $d^n$  and  $d^{n\pm 1}\bar{\text{L}}$  states) and small or even negative charge excitation gap  $\Delta_{\text{CT}}$  (refs 1,2,28,35). In these materials, the role of the lower Hubbard band is replaced by the oxygen states, which in turn implies a very asymmetric physical character for the doped holes (mainly in oxygen levels) and doped electrons (mainly in transition metal *d* levels), for example, correlated metal LaNiO<sub>3</sub> (LNO). With the original motivation to create a cuprate-like electronic and orbital structures<sup>6,36,37</sup>, LNO-based perovskite heterostructures have attracted continuous interest<sup>6,16–22,38–43</sup> in spite of the intriguing bulk properties

of charge-transfer materials. However, experimentally very little is known about the Mott carrier redistribution and their electronic reconfigurations at the heterointerface between MHI and CTM<sup>20–22</sup>.

Towards this goal, we have synthesized and investigated a prototypical MHI/CTM heterostructure (2 u.c. LaTiO<sub>3</sub> +  $\delta/2$  u.c. LaNiO<sub>3</sub>)  $\times 10$  (2LTO/2LNO thereafter, u.c. = unit cells,  $\delta \sim 0.34$  is the concentration of oxygen excess from the ideal Ti<sup>3+</sup> state). The resulting 2LTO/2LNO heterostructure exhibits an exotic Mott ground state. To quantify this phenomenon, we investigated the interfacial charge transfer from Ti to Ni sites and the reconstruction of the electronic structure by resonant soft X-ray absorption spectroscopy (XAS) at Ti, Ni  $L_{2,3}$  – and O K-edges combined with X-ray photoemission spectroscopy (XPS), electrical transport and first-principles calculations. X-ray linear dichroism (XLD) spectroscopy was carried out to reveal the orbital polarization and unexpected Ni  $e_g$  band splitting. Our findings highlight how the control over charge at the interface can be effectively used to create exotic electronic, orbital and spin states.

## Results

**Interfacial charge transfer.** As shown in Fig. 1, driven by the difference between Fermi levels  $E_{\text{F}}$  or chemical potentials in constituent layers across the junction 2LTO/2LNO (see Fig. 1a and Supplementary Fig. 1), in a conventional view the charge redistributes near the interface. As the components of 2LTO/2LNO superlattice (SL), the electronic configuration of CTM LaNi<sup>3+</sup>O<sub>3</sub> is a mixture of low-spin  $3d^7$  and high-spin  $3d^8\bar{\text{L}}$  states with the Fermi energy passing through the strongly mixed Ni–O valence states<sup>44,45</sup>, whereas as an archetypal MHI ( $\sim 0.2$  eV gap) bulk LaTi<sup>3+</sup>O<sub>3</sub> has only one electron ( $3d^1$ ) occupying the lower Hubbard band<sup>46,47</sup> and its Fermi energy level  $E_{\text{F}}$  is much higher than that of LNO ( $\sim 2$  eV difference)<sup>48</sup>, as schematically shown in Fig. 1b. By aligning the interfacial bands with respect to the continuing oxygen *p* states on either side of the interface<sup>20,49</sup>, the resulting Ti  $3d$  band energy position becomes significantly higher than the Fermi energy of the LNO; this in turn implies a one-way charge redistribution from the Ti  $3d$  band of LTO into the partially filled Ni *d* and O *p* states of LNO. Recent density functional theory (DFT + *U*) calculations<sup>20</sup> further tested this naive picture and suggested a full electron charge transfer, that is, Ti  $d^1 + \text{Ni } d^7 \rightarrow \text{Ti } d^0 + \text{Ni } d^8$  (Fig. 1c). On the other hand, as the experimental electronic configuration of LNO is a mixture of Ni  $d^7$  and  $d^8\bar{\text{L}}$  states, the charge transfer may also result in the appearance of additional interfacial electronic states, that is, Ti  $d^1 + \text{Ni } d^8\bar{\text{L}} \rightarrow \text{Ti } d^0 + \text{Ni } d^8$  and Ti  $d^1 + \text{Ni } d^8\bar{\text{L}} \rightarrow \text{Ti } d^0 + \text{Ni } d^9\bar{\text{L}}$ .

To investigate the experimental veracity of the theory, we measured the electronic structures of Ti and Ni, to track the charge transfer by element-specific XAS in total fluorescence yield mode (with the bulk probing depth) and by *in-situ* XPS. As seen in Fig. 2a, the features of the Ti  $L_{2,3}$ -edge in the 2LTO/2LNO sample show excellent agreement with the Ti<sup>4+</sup> charge and are remarkably different from the spectra of Ti<sup>3+</sup>. This result provides a strong evidence for the occurrence of the charge-transfer Ti  $d^{(1-2\delta)} \rightarrow \text{Ti } d^0$  and implies that almost all of the  $L_{2g}$  electrons from Ti sites are transferred elsewhere. The flow of the charge is further verified by the complimentary XAS measurements at the Ni  $L_{2,3}$ -edge, which clearly shows a strong increase of the Ni charge state, that is, Ni  $d^7 \rightarrow \text{Ni } d^{(8-2\delta)}$  (see Fig. 2b). A comparison with the bulk reference spectra of Ni<sup>2+</sup> (double peaks at  $\sim 870.2$  and  $871.2$  eV) and Ni<sup>3+</sup> (single main peak at  $\sim 871.6$  eV) attests that in the 2LTO/2LNO SL the Ni final state is indeed a mixture of Ni<sup>2+</sup>/Ni<sup>3+</sup> (double

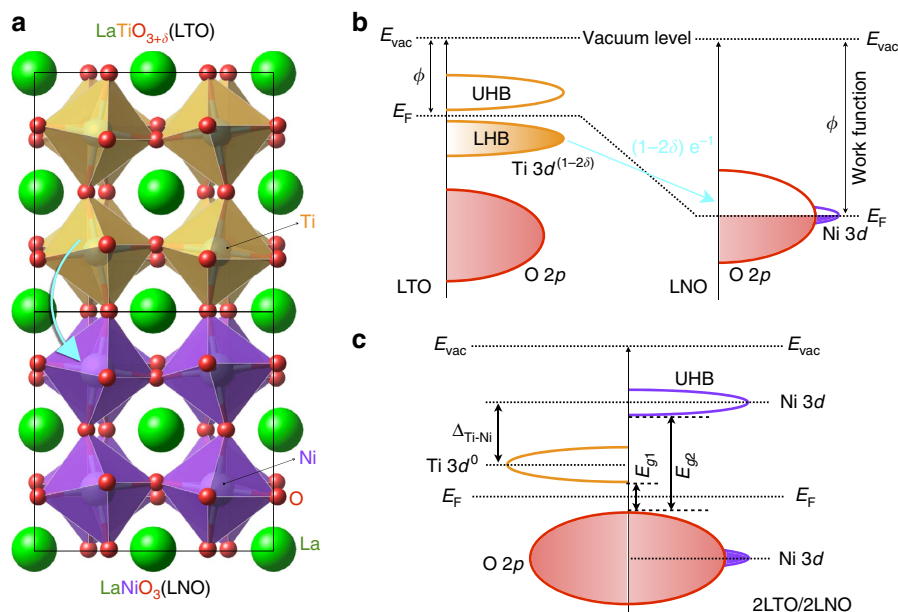


**Figure 1 | Crystal and band structures of 2LTO/2LNO.** (a) Schematic view of the atomic arrangement. Sketch of the energy bands before (b) and after (c) the formation of 2LTO/2LNO interface. The cyan solid arrows in **a, b** indicate the direction of interfacial charge transfer (electron,  $e^{-1}$ ) from Ti to Ni sites. Here,  $E_{g1}$  (or  $E_{g2}$ ), charge gap between the highest occupied state (a mixture of oxygen 2p and Ni 3d states<sup>20</sup>) and the bottom of empty Ti 3d (or Ni 3d) state;  $\Delta_{\text{Ti-Ni}}$ , relative energy difference between empty Ti and Ni 3d states; LHB, lower Hubbard band; UHB, upper Hubbard band.

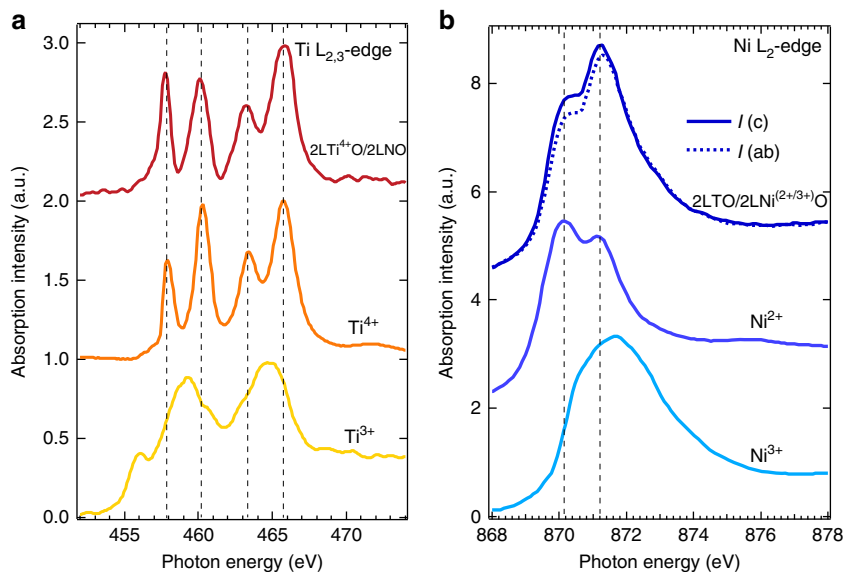


**Figure 2 | XAS of 2LTO/2LNO.** (a) Ti  $L_{2,3}$ -edge. The reference spectra for  $\text{Ti}^{4+}$  and  $\text{Ti}^{3+}$  were measured on a  $\text{SrTi}^{4+}\text{O}_3$  single crystal and  $\text{YTi}^{3+}\text{O}_3$  film ( $\sim 100$  nm on  $\text{TbScO}_3$  substrate<sup>59</sup>), respectively. (b) Ni  $L_{2,3}$ -edge. The reference samples are bulk  $\text{Ni}^{2+}\text{O}$  and  $\text{LaNi}^{3+}\text{O}_3$ . Out-of-plane ( $I(c)$ , dark blue solid line,  $E \parallel c$  and  $E$  is the linear polarization vector of the photon) and in-plane ( $I(ab)$ , dark blue dashed line,  $E \parallel ab$ ) linearly polarized X-ray were used to measure XAS of 2LTO/2LNO at Ni  $L_{2,3}$ -edge. Black dashed lines are guidelines for peak positions. All spectra were collected and repeated more than two times with bulk-sensitive total fluorescence yield (TFY) detection mode at room temperature.

peaks), which is also affirmed by the calculated XAS lineshape dependence on the Ni electronic configuration (see Supplementary Fig. 2). To further corroborate these findings, the interfacial charge-transfer phenomenon was studied by measuring the core-level electronic structures of Ti and Ni with *in-situ* XPS (see Supplementary Fig. 3); as determined by XPS, the resulting charge states of Ni and Ti in the 2LTO/2LNO sample are in excellent agreement with those obtained by XAS at Ti  $L_{2,3}$ - and Ni  $L_{2,3}$ -edges. Moreover, as revealed by the

angle-dependent (*ex situ*) XPS (see Supplementary Fig. 4), the pronounced  $\text{Ni}^{2+}$  peak near the interface of metallic 2LTO/8LNO (see Supplementary Fig. 5) further confirmed the interfacial charge transfer from Ti to Ni sites.

**Electronic reconstruction.** With the confirmed large interfacial charge transfer from Ti to Ni sites, an important question arises: how does the interfacial charge transfer alter the fundamental

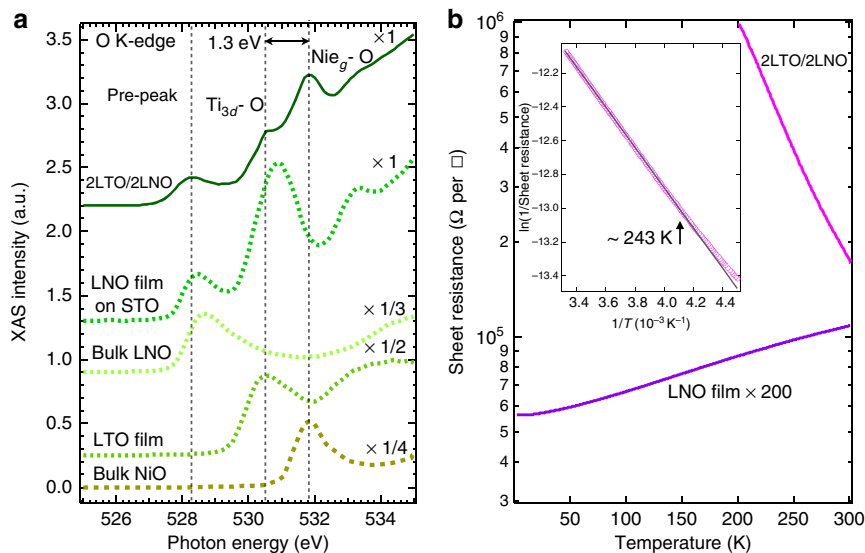


**Figure 3 | Oxygen K-edge spectra and electrical transport of 2LTO/2LNO.** (a) Normalized XAS spectra at O K-edge. The black dashed lines indicate the assignments of three key features: the pre-peak ( $\sim 528.5$  eV) and hybridized Ti  $3d$ -O ( $\sim 530.5$  eV) and Ni  $e_g$ -O ( $\sim 531.8$  eV) states by comparing with the spectra of four reference samples LaNi $^{3+}$ O $_3$  film (10 u.c. on SrTiO $_3$  substrate), bulk LaNi $^{3+}$ O $_3$ , LaTi $^{3+}$ O $_3$  film (20 u.c. on TbScO $_3$  substrate $^{59}$ ) and bulk Ni $^{2+}$ O (the data of NiO was adapted from ref. 60). (b) Temperature-dependent sheet resistances of the SL 2LTO/2LNO and the reference LaNiO $_3$  film (20 u.c.). It is noteworthy that the sheet resistance of LNO film is  $\times 200$ . Inset: resulting fit of the conductance of 2LTO/2LNO (black solid line) yielding an activation gap  $E_{g1} \sim 0.2 \pm 0.01$  eV (ref. 61).

physical properties (that is, electronic configuration and band structure) of the 2LTO/2LNO SL? First, we discussed the emergent electronic configuration. As mentioned above, the channels of interfacial charge-transfer Ti  $d^1 + \text{Ni } d^7 \rightarrow \text{Ti } d^0 + \text{Ni } d^8$  and Ti  $d^1 + \text{Ni } d^8 \rightarrow \text{Ti } d^0 + \text{Ni } d^8$  are both open at the interface. Experimentally, owing to the strong hybridization between Ni  $3d$  states and oxygen  $2p$  states at the Fermi level, XAS at O K-edge becomes another important way to probe the charge states of Ni and Ti mixed with ligand holes. As seen in Fig. 3a and Supplementary Fig. 6, in 2LTO/2LNO the oxygen K-edge spectra clearly show a characteristic low-energy pre-peak at  $\sim 528.5$  eV, which arises from the ligand holes $^{18}$ . In sharp contrast, a direct comparison with the LTO and LNO reference samples immediately shows that the pre-peak at the 2LTO/2LNO interface is strongly suppressed due to the filling oxygen ligand holes with the transferred electrons from Ti sites (also see Supplementary Fig. 6). Based on the absence of the pre-peak feature in the LaTi $^{3+}$ O $_3$  and Ni $^{2+}$ O reference samples, these data imply that the strong suppression of the pre-peak intensity results from the filling of holes on oxygen by the interfacial charge transfer into the Ni  $d$ -band. As a result, this process induces the formation of the  $d^8$  state and the strong suppression of the  $d^8$  configuration. In addition, we point out at the expected difference between the theory (full charge transfer of one electron) $^{20}$  and the experimental observation of less than one electron transfer, that is,  $(1 - 2\delta)$  electron; the observed deviation from the full charge transfer in theory is due to the reduced electron filling from unity,  $2\delta$  of the Ti  $d$ -band. Combined with the mixed  $d^7$  and  $d^8$  ground state of bulk LNO, this factor results in the observed peculiar electronic configuration of  $d^8$ ,  $d^7$  and  $d^8$  states, which appears at the interfacial NiO $_2$  layer in 2LTO/2LNO.

Next, we discuss the reconstructed band structure at the interface. Because of the observed strong reconstruction of electronic configuration, it is natural to anticipate a similarly strong modification of the band structure near the interface. As predicted by the theory $^{20}$  and illustrated in Fig. 1c, two opening gaps  $E_{g1}$  and  $\Delta_{\text{Ti-Ni}}$  are expected to appear at the interface. First, we estimated a magnitude of the charge gap  $E_{g1}$  by measuring the

temperature-dependent electrical transport properties of the 2LTO/2LNO and LNO reference films. As immediately seen in Fig. 3b, the LNO thin film grown at the same conditions as the SL shows a metallic bulk-like behaviour ( $\sim 280 \Omega$  per  $\square$  at 2 K) from room temperature down to 2 K. In sharp contrast, the SL 2LTO/2LNO displays a highly insulating behaviour with a very large sheet resistance increasing from  $\sim 175 \text{ k}\Omega$  per  $\square$  at 300 K to  $\sim 1 \text{ M}\Omega$  per  $\square$  at 200 K, exceeding the measurement range of the transport setup. This insulating behaviour of the 2LTO/2LNO implies the charge excitations gap opening in 2LTO/2LNO. The resulting fit to the transport data shown in inset of Fig. 3b yields a value of  $E_{g1} \sim 0.20 \pm 0.01$  eV; this is in accord with the theoretical prediction of the  $\sim 0.4$  eV charge-transfer gap $^{20}$ .

Next, we estimate the value of the gap  $\Delta_{\text{Ti-Ni}}$  between empty Ti  $t_{2g}$  and Ni  $e_g$  bands by measuring XAS of the 2LTO/2LNO film at O K-edge. In a simple ionic model, the configuration of oxygen is O  $1s^2 2s^2 2p^6$  and thus the transition  $1s \rightarrow 2p$  is blocked in the absorption process, because it is a fully occupied  $2p$  shell for the O ion. In real materials, however, owing to the strong hybridization the covalent bonding between the transition metal ion and oxygen can introduce a sizable spectral weight of oxygen  $2p$  character in the total unoccupied density of states $^{50-53}$ . As a result, O K-edge XAS provides a complimentary way to probe the relative energy position of the TM ion. We also point out that in comparison with the L $_{2,3}$ -edge XAS reflecting the absorption process for the specific TM ion, O K-edge provides a convenient way to measure the relative energy position of the unoccupied bands of both TM ions (Ti and Ni) present in the 2LTO/2LNO heterostructure $^{52}$ . A direct comparison with the reference samples allows to assign the two peaks at  $\sim 530.5$  and  $\sim 531.8$  eV shown in Fig. 3a to the hybridized oxygen  $2p$  with Ti  $3d$  and Ni  $e_g$  bands, respectively, and then to extract the value of the Mott gap  $\Delta_{\text{Ti-Ni}} \sim 1.3$  eV. Assuming that the bandwidth of Ti  $3d$ -O and Ni  $e_g$ -O bands is roughly the same (see Fig. 3a) and with the known value of  $E_{g1} \sim 0.2$  eV the estimated value of the correlated gap  $E_{g2} = (E_{g1} + \Delta_{\text{Ti-Ni}})$  is  $\sim 1.5$  eV, this value is in a remarkable agreement with the theoretically predicted value of  $\sim 1.5$  eV (ref. 20). The above observation of the two gaps opening

in the excitation spectrum lends strong support to the notion of a strong modification of the band structure at the interface triggered by the redistribution of correlated charges. It is also noted that some additional contributions (for example, disorder effect, electron–electron interactions and charge/spin order)<sup>44,54,55</sup> may be involved in the enhanced carrier localization of 2LTO/2LNO. However, their contributions are not dominant in comparison with the large  $\sim 1.5$  eV correlated gap of 2LTO/2LNO. As demonstrated by the angle-dependent XPS on 2LTO/8LNO (see Supplementary Fig. 4), the formation of  $\text{Ni}^{2+}$  accompanied with the strongly suppressed density of states near the Fermi energy level is primarily driven by the interfacial charge transfer from Ti to Ni sites.

**Orbital reconstruction.** With the established strongly altered  $d$ -band filling on Ni and Ti, we investigated the orbital properties of these engineered states on Ni sites. To this end, the orbital polarization has been measured by XLD<sup>16,18,19,56</sup> on several LNO-based heterostructures and the result for the LTO/LNO SL is shown in Fig. 4a. Based on the measured electronic state of Ni, one can anticipate that contribution to the XLD signal on Ni  $L_2$ -edge arises largely from the unoccupied Ni  $d_{x^2-y^2}$  ( $I(ab)$ ) and  $d_{3z^2-r^2}$  ( $I(c)$ ) states. As illustrated in Fig. 4a, those orbital configurations can be probed with in-plane ( $E \parallel ab$ ,  $E$  is the polarization vector of the photon) and out-of-plane ( $E \parallel c$ ) linearly polarized photons, respectively. In a good agreement with

this expectation, the XLD spectra shown in Fig. 4a show an ample degree of orbital polarization of  $\sim 9.3\%$  at  $L_2$ -edge with the  $d$ -electron occupancy  $n_{d_{x^2-y^2}} > n_{d_{3z^2-r^2}}$  consistent with the first principle calculation prediction of  $\sim 9\%$  (see Calculation details in Methods).

The surprising feature of the XLD data for 2LTO/2LNO is the presence of  $e_g$  band splitting (Fig. 4b,c) that was not observed in tensile-strained ultra-thin LNO films or SL (1 u.c.)LNO/(1 u.c.)LaAlO<sub>3</sub> (refs 18,19). It is noteworthy that the band splitting is generally estimated by the peak energy shift of XAS (between  $I(ab)$  and  $I(c)$ ) with linearly polarized photons and the lineshape of XLD ( $I(ab)-I(c)$ ) with multiple peak features does not infer the size of the band splitting directly. In the case of 2LTO/2LNO, however, small tensile strain of  $+1.04\%$  causes the sizable  $e_g$  band splitting. Specifically, as seen in inset of Fig. 4b,c, a direct inspection of the energy position for in-plane ( $\sim 853.15$  eV) and out-of-plane ( $\sim 853.0$  eV) absorption curves reveal that the out-of-plane absorption is  $\sim 0.15$  eV (0.12 eV) lower in energy than the in-plane absorption at Ni  $L_3(L_2)$ -edge. The difference implies the  $e_g$  band splitting  $\Delta e_g \sim 0.15$  eV between the states with Ni  $d_{x^2-y^2}$  and  $d_{3z^2-r^2}$  orbital character, as schematically illustrated in Fig. 4d,e. This observation lends a strong support to that recently predicted by theory (see Calculation details in Methods), that both band splitting and orbital polarization arise from the structural distortions at the interface. The apical oxygen atom of out-of-plane Ni–O–Ti bond approaches Ti and leaves away from Ni atoms, whereas the in-plane Ni–O bond length is changed a

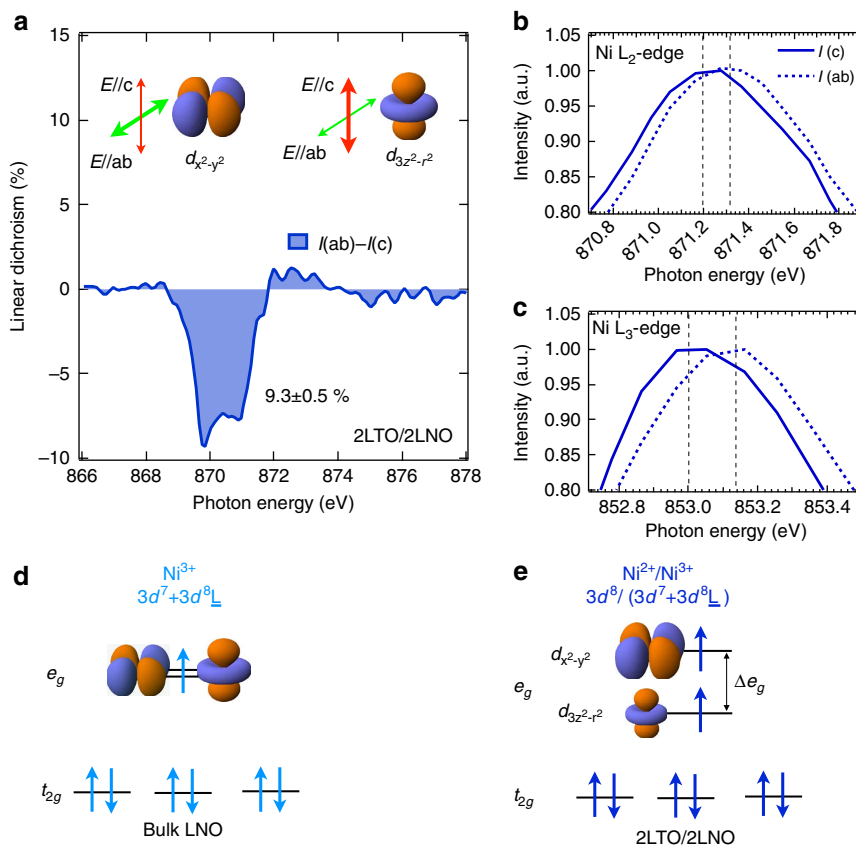


**Figure 4 | Linear dichroism and reconstructed states.** (a) XLD ( $I(ab) - I(c)$ ) of 2LTO/2LNO interface (extracted from Fig. 2b). Green (in-plane) and red (out-of-plane) arrows label the direction of linear polarization vector ( $E$ ) of the photon. (b,c) XAS of 2LTO/2LNO at Ni  $L_{2,3}$ -edge showing the Ni  $e_g$  band splitting ( $\sim 0.12$  for  $L_2$  and  $0.15$  eV for  $L_3$ , respectively) of  $d_{3z^2-r^2}$  (lower) and  $d_{x^2-y^2}$  (higher) orbitals. Black dashed lines are guidelines for peak centre positions. (d,e) Sketch of the engineered electronic, orbital and spin states via interfacial charge transfer for bulk LNO<sup>18</sup> and SL 2LTO/2LNO, respectively. In SL 2LTO/2LNO, it forms peculiar electronic configuration (Ni  $3d^7$ ,  $3d^8$  and  $3d^8\downarrow$ ), orbital polarization ( $n_{d_{x^2-y^2}} > n_{d_{3z^2-r^2}}$ ) and  $e_g$  band splitting ( $\Delta e_g \sim 0.15$  eV). Blue arrows indicate the spin configurations of Ni sites.

little and smaller than the out-of-plane Ni–O bond length. This extended out-of-plane Ni–O bond leads to the lowering of Ni  $d_{3z^2-r^2}$  central band energy; on the other hand, it also obviously weakens the hybridization between O  $2p$  and Ni  $d_{3z^2-r^2}$  bands with suppressed virtual electron hopping. Therefore, the larger hybridization between O  $2p$  and Ni  $d_{x^2-y^2}$  bands results in a higher electron occupancy at higher Ni  $d_{x^2-y^2}$  (minority spin) orbital band  $n_{d_{x^2-y^2}} > n_{d_{3z^2-r^2}}$ , which is very unusual.

In conclusion, by synthesizing the 2LTO/2LNO interface as a prototypical system, we investigated the reconstruction of the local electronic structure on Ni and Ti at the interface between a doped MHI and a charge-transfer metal. Our findings reveal the occurrence of large charge transfer from the Ti to Ni sites across the interface that results in the unusual electronic configurations of Ni  $3d$  electrons and lead to the strong modification of the band structure in the vicinity of the interface. In addition, the XLD data show the presence of the large orbital polarization and energy splitting of the Ni  $e_g$  band at the vicinity of the interface characteristic of the Jahn–Teller distortion absent in either bulk rare-earth nickelates or other ultra-thin LNO-based heterojunctions. We anticipate that these results will pave the way for follow-up theoretical and experimental work with other important classes of charge-transfer interfaces, to establish a discovery platform for exotic many-body quantum phenomena.

## Methods

**Experiment details.** High-quality SLs (2LTO/*m.u.c.* LNO)  $\times 10$  ( $n = 2$  and  $8$ , 2LTO/2LNO and 2LTO/8LNO) and reference samples were epitaxially grown by pulsed laser deposition on  $5 \times 5 \times 0.5$  mm<sup>3</sup> (001)-oriented single crystal substrates (LaAlO<sub>3</sub>)<sub>0.3</sub>–(Sr<sub>2</sub>AlTaO<sub>6</sub>)<sub>0.7</sub> (cubic,  $a = 3.87$  Å), using a KrF excimer laser operating at  $\lambda = 248$  nm and 2 Hz pulse rate with  $2$  J cm<sup>-2</sup> fluence. The layer-by-layer growth was monitored by *in-situ* high-pressure reflection high-energy electron diffraction (see Supplementary Fig. 1). To match the growth conditions for both LaTiO<sub>3+ $\delta$</sub>  and LNO, the SLs 2LTO/2LNO and 2LTO/8LNO were grown under oxygen pressure  $\sim 50$  mTorr and the temperature of the substrates was held at 580 °C during the growth. After growth, all samples were cooled at  $\sim 15$  °C min<sup>-1</sup> rate to room temperature keeping oxygen pressure constant. A Mg anode was used for *in-situ* XPS measurements with double-pass cylindrical mirror analysers (STAIB Instruments) at room temperature, whereas for *ex-situ* angle-dependent XPS measurements with a hemispherical electron analyser an Al anode with monochromator (PHI VersaProbe II) was applied. The sheet resistances of the films were measured in van-der-Pauw geometry by Physical Properties Measurement System (Quantum Design) from 300 to 2 K. XAS/XLD with total fluorescence yield mode and X-ray diffraction measurements (room temperature) were carried out at the 4-ID-C and 6-ID-B beamlines, respectively, of the Advanced Photon Source (Argonne National Laboratory).

**Calculation details.** Calculated XAS at Ni L<sub>2,3</sub>- and O K-edges of rhombohedral (R-3cH space group) LNO<sup>57</sup> were carried out with the finite difference method near-edge structure code<sup>58</sup>. In finite difference method near-edge structure calculations we used the full-multiplet scattering (Green function) mode with a large cluster radius of 6 Å around the absorbing Ni atom. The XAS calculations were performed for various Ni  $3d^xL^y$  ( $7 < x \leq 8$ ) configurations of LNO (see Supplementary Fig. 2). To confirm the consistency of the calculated XAS spectra, we also performed XAS calculations using the multi-electron time-dependent DFT (+ $U$ ) with an on-site Coulomb energy on Ni of 6 eV. On the other hand, in the calculation of SL 2LaTiO<sub>3</sub>/2LNO by the DFT +  $U$  method ( $U_{\text{Ni}} = 6$  eV and  $U_{\text{Ti}} = 4$  eV), the orbital polarization of unoccupied states is  $[(2 - n_{d_{x^2-y^2}}) - (2 - n_{d_{3z^2-r^2}})] / [(2 - n_{d_{x^2-y^2}}) + (2 - n_{d_{3z^2-r^2}})] \sim -9\%$ , where  $n_{d_{x^2-y^2}}$  and  $n_{d_{3z^2-r^2}}$  are total electron occupancy (spin up plus spin down) with the  $d_{x^2-y^2}$  and  $d_{3z^2-r^2}$  orbital characters of the  $e_g$  band, respectively; it is noteworthy that the central energy position of  $d_{x^2-y^2}$  band is higher than that of the  $d_{3z^2-r^2}$  band (personal communication with A.J. Millis and H. Chen).

## References

- Imada, M., Fujimori, A. & Tokura, Y. Metal-insulator transitions. *Rev. Mod. Phys.* **70**, 1039–1263 (1998).
- Khomskii, D. *Transition Metal Compounds* (Cambridge Univ. Press, 2014).
- Tokura, Y. & Nagaosa, N. Orbital physics in transition-metal oxides. *Science* **288**, 462–468 (2000).
- Ahn, C. H. *et al.* Electrostatic modification of novel materials. *Rev. Mod. Phys.* **78**, 1185–1212 (2006).
- Hwang, H. Y. *et al.* Emergent phenomena at oxide interfaces. *Nat. Mater.* **11**, 103–113 (2012).
- Chakhalian, J., Freeland, J. W., Millis, A. J., Panagopoulos, C. & Rondinelli, J. M. Colloquium: emergent properties in plane view: strong correlations at oxide interfaces. *Rev. Mod. Phys.* **86**, 1189–1202 (2014).
- Chakhalian, J., Millis, A. J. & Rondinelli, J. Whither the oxide interface. *Nat. Mater.* **11**, 92–94 (2012).
- Mannhart, J. & Schlom, D. G. Oxide interfaces—an opportunity for electronics. *Science* **327**, 1607–1611 (2010).
- Coey, J. M. D., Ariando & Pickett, W. E. Magnetism at the edge: new phenomena at oxide interfaces. *MRS Bull.* **38**, 1040–1047 (2013).
- Schlom, D. G. *et al.* Strain tuning of ferroelectric thin films. *Annu. Rev. Mater. Res.* **37**, 589–626 (2007).
- Stemmer, S. & Allen, S. J. Two-dimensional electron gases at complex oxide interfaces. *Annu. Rev. Mater. Res.* **44**, 151–171 (2014).
- Bhattacharya, A. & May, S. J. Magnetic oxide heterostructures. *Annu. Rev. Mater. Res.* **44**, 65–90 (2014).
- Zubko, P., Gariglio, S., Gabay, M., Ghosez, P. & Triscone, J. Interface physics in complex oxide heterostructures. *Annu. Rev. Condens. Matter Phys.* **2**, 141–165 (2011).
- Ngai, J. H., Walker, F. J. & Ahn, C. H. Correlated oxide physics and electronics. *Annu. Rev. Mater. Res.* **44**, 1–17 (2014).
- Chakhalian, J. *et al.* Orbital reconstruction and covalent bonding at an oxide interface. *Science* **318**, 1114–1117 (2007).
- Benckiser, E. *et al.* Orbital reflectometry of oxide heterostructures. *Nat. Mater.* **10**, 189–193 (2011).
- Liu, J. *et al.* Quantum confinement of Mott electrons in ultrathin LaNiO<sub>3</sub>/LaAlO<sub>3</sub> superlattices. *Phys. Rev. B* **83**, 161102 (R) (2011).
- Chakhalian, J. *et al.* Asymmetric orbital-lattice interactions in ultrathin correlated oxide films. *Phys. Rev. Lett.* **107**, 116805 (2011).
- Freeland, J. *et al.* Orbital control in strained ultra-thin LaNiO<sub>3</sub>/LaAlO<sub>3</sub> superlattices. *Europhys. Lett.* **96**, 57004 (2011).
- Chen, H., Millis, A. & Marianetti, C. Engineering correlation effects via artificially designed oxide superlattices. *Phys. Rev. Lett.* **111**, 116403 (2013).
- Chen, H. *et al.* Modifying the electronic orbitals of nickelate heterostructures via structural distortions. *Phys. Rev. Lett.* **110**, 186402 (2013).
- Disa, A. *et al.* Orbital engineering in symmetry-breaking polar heterostructures. *Phys. Rev. Lett.* **114**, 026801 (2015).
- Stormer, H. L., Tsui, D. & Gossard, A. The fractional quantum Hall effect. *Rev. Mod. Phys.* **71**, S298–S305 (1999).
- Marie, X. & Balkan, N. *Semiconductor Modeling Techniques* (Springer, 2012).
- Gertner, J. *The Idea Factory: Bell Labs and the Great Age of American Innovation* (The Penguin Press, 2012).
- Schubert, E. F. Delta doping of III-V compound semiconductors: fundamentals and device applications. *J. Vac. Sci. Technol. A* **8**, 2980 (1990).
- Sze, S. M. & Ng, K. *Physics of Semiconductor Devices, Third Edition* (John Wiley & Sons, Inc., 2007).
- Zaanen, J., Sawatzky, G. & Allen, J. Band gaps and electronic structure of transition-metal compounds. *Phys. Rev. Lett.* **55**, 418–421 (1985).
- Lee, W.-C. & MacDonald, A. H. Modulation doping near Mott-insulator heterojunctions. *Phys. Rev. B* **74**, 075106 (2006).
- Charlebois, M., Hassan, S. R., Karan, R., Sénéchal, D. & Tremblay, A.-M. S. Mott p-n junctions in layered materials. *Phys. Rev. B* **87**, 035137 (2013).
- Oka, T. & Nagaosa, N. Interfaces of correlated electron systems: proposed mechanism for colossal electroresistance. *Phys. Rev. Lett.* **95**, 266403 (2005).
- Okamoto, S. Nonequilibrium transport and optical properties of model metal-Mott-insulator-metal heterostructures. *Phys. Rev. B* **76**, 035105 (2007).
- Yonemitsu, K., Maeshima, N. & Hasegawa, T. Suppression of rectification at metal-Mott insulator interfaces. *Phys. Rev. B* **76**, 235118 (2007).
- Al-Hassanieh, K. A., Rincón, J., Alvarez, G. & Dagotto, E. Spin Andreev-like reflection in metal-Mott insulator heterostructures. *Phys. Rev. Lett.* **114**, 066401 (2015).
- Khomskii, D. & Sawatzky, G. Interplay between spin, charge and orbital degrees of freedom in magnetic oxides. *Solid State Commun.* **102**, 87–99 (1997).
- Chaloupka, J. & Khaliullin, G. Orbital order and possible superconductivity in LaNiO<sub>3</sub>/LaMO<sub>3</sub> superlattices. *Phys. Rev. Lett.* **100**, 016404 (2008).
- Hansmann, P. *et al.* Turning a nickelate Fermi surface into a cupratelike one through heterostructuring. *Phys. Rev. Lett.* **103**, 016401 (2009).
- Hoffman, J. *et al.* Charge transfer and interfacial magnetism in (LaNiO<sub>3</sub>)<sub>n</sub>/(LaMnO<sub>3</sub>)<sub>2</sub> superlattices. *Phys. Rev. B* **88**, 144411 (2013).
- Kaiser, A. M. *et al.* Suppression of near-Fermi level electronic states at the interface in a LaNiO<sub>3</sub>/SrTiO<sub>3</sub> superlattice. *Phys. Rev. Lett.* **107**, 116402 (2011).
- Son, J., LeBeau, J., Allen, S. & Stemmer, S. Conductivity enhancement of ultrathin LaNiO<sub>3</sub> films in superlattices. *Appl. Phys. Lett.* **97**, 202109 (2010).
- May, S. J., Santos, T. S. & Bhattacharya, A. Onset of metallic behavior in strained (LaNiO<sub>3</sub>)<sub>n</sub>/(SrMnO<sub>3</sub>)<sub>2</sub> superlattices. *Phys. Rev. B* **79**, 115127 (2009).

42. Rojas Sánchez, J. C., Nelson-Cheeseman, B., Granada, M., Arenholz, E. & Steren, L. B. Exchange-bias effect at  $\text{La}_{0.75}\text{Sr}_{0.25}\text{MnO}_3/\text{LaNiO}_3$  interfaces. *Phys. Rev. B* **85**, 094427 (2012).
43. Han, M. J., Wang, X., Marianetti, C. A. & Millis, A. J. Dynamical mean-field theory of nickelate superlattices. *Phys. Rev. Lett.* **107**, 206804 (2011).
44. Scherwitzl, R. *et al.* Metal-insulator transition in ultrathin  $\text{LaNiO}_3$  films. *Phys. Rev. Lett.* **106**, 246403 (2011).
45. Garca, J., Blasco, J., Proietti, M. G. & Benfatto, M. Analysis of the x-ray-absorption near-edge-structure spectra of  $\text{La}_{1-x}\text{Nd}_x\text{NiO}_3$  and  $\text{LaNi}_{1-x}\text{Fe}_x\text{O}_3$  perovskites at the nickel K edge. *Phys. Rev. B* **52**, 15823–15828 (1995).
46. Mochizuki, M. & Imada, M. Orbital physics in the perovskite Ti oxides. *New J. Phys.* **6**, 154 (2004).
47. Okimoto, Y., Katsufuji, T., Okada, Y., Arima, T. & Tokura, Y. Optical spectra in  $(\text{La},\text{Y})\text{TiO}_3$ : variation of Mott-Hubbard gap features with change of electron correlation and band filling. *Phys. Rev. B* **51**, 9581–9588 (1995).
48. Greiner, M. T., Chai, L., Helander, M., Tang, W. & Lu, Z. Transition metal oxide work functions: the influence of cation oxidation state and oxygen vacancies. *Adv. Funct. Mater.* **22**, 4557–4568 (2012).
49. Kleibecker, J. *et al.* Electronic reconstruction at the isopolar  $\text{LaTiO}_3/\text{LaFeO}_3$  interface: an X-Ray photoemission and density-functional theory study. *Phys. Rev. Lett.* **113**, 237402 (2014).
50. Wu, Z. Y., Ouyard, G., Gressier, P. & Natoli, C. R. Ti and O K edges for titanium oxides by multiple scattering calculations: comparison to XAS and EELS spectra. *Phys. Rev. B* **55**, 10382–10391 (1997).
51. Mossaneck, R. J. O. *et al.* Effects of Ni vacancies and crystallite size on the O 1s and Ni 2p x-ray absorption spectra of nanocrystalline NiO. *J. Phys. Condens. Matter* **25**, 495506 (2013).
52. Cho, D., Song, S., Kim, U., Lee, H. & Hwang, C. Spectroscopic investigation of the hole states in Ni-deficient NiO films. *J. Mater. Chem. C* **1**, 4334–4338 (2013).
53. de Groot, F. M. F. *et al.* Oxygen 1 s x-ray-absorption edges of transition-metal oxides. *Phys. Rev. B* **40**, 5715–5723 (1989).
54. Moon, E. J. *et al.* Strain-dependent transport properties of the ultra-thin correlated metal,  $\text{LaNiO}_3$ . *New J. Phys.* **13**, 073037 (2011).
55. King, P. D. C. *et al.* Atomic-scale control of competing electronic phases in ultrathin  $\text{LaNiO}_3$ . *Nat. Nanotechnol.* **9**, 443–447 (2014).
56. Wu, M. *et al.* Strain and composition dependence of orbital polarization in nickel oxide superlattices. *Phys. Rev. B* **88**, 125124 (2013).
57. Garca-Muñoz, J. L., Rodríguez-Carvajal, J., Lacorre, P. & Torrance, J. B. Neutron-diffraction study of  $\text{RNiO}_3$  (R = La, Pr, Nd, Sm): electronically induced structural changes across the metal-insulator transition. *Phys. Rev. B* **46**, 4414–4425 (1992).
58. Bunău, O. & Joly, Y. Self-consistent aspects of x-ray absorption calculations. *J. Phys. Condens. Matter* **21**, 345501 (2009).
59. Kareev, M. *et al.* Metallic conductance at the interface of tri-color titanate superlattices. *Appl. Phys. Lett.* **103**, 231605 (2013).
60. Lin, F. *et al.* Phase evolution for conversion reaction electrodes in lithium-ion batteries. *Nat. Commun.* **5**, 3358 (2014).
61. Middey, S. *et al.* Epitaxial growth of (111)-oriented  $\text{LaAlO}_3/\text{LaNiO}_3$  ultra-thin superlattices. *Appl. Phys. Lett.* **101**, 261602 (2012).

## Acknowledgements

We acknowledge numerous fruitful discussions with Andrew Millis and Hanghui Chen. J.C. and X.L. were supported by the Department of Energy grant DE-SC0012375 for synchrotron work at the Advanced Photon Source and material synthesis. D.M. was primarily supported by the Gordon and Betty Moore Foundation EPiQS Initiative through grant number GBMF4534. Y.C. and S.M. were supported by the DOD-ARO under grant number 0402-17291. This research used resources of the Advanced Photon Source, a US Department of Energy (DOE) Office of Science User Facility operated for the DOE Office of Science by Argonne National Laboratory under contract number DE-AC02-06CH11357.

## Author contributions

Y.C. and J.C. designed the experiments. Y.C., X.L. and S.M. measured the electrical transport. Y.C. and M.K. collected the XPS data. Y.C., X.L., S.M., D.M., J.K. and P.R. measured the X-ray diffraction. J.W.F. acquired the XAS data. D.C. and J.C. carried out the theoretical calculations. M.K. and Y.C. prepared the samples. Y.C. and J.C. analysed the data. All authors discussed the results. Y.C., D.M., D.C. and J.C. wrote the manuscript with input from all authors. This work was supervised by J.C.

## Additional information

**Supplementary Information** accompanies this paper at <http://www.nature.com/naturecommunications>

**Competing financial interests:** The authors declare no competing financial interests.

**Reprints and permission** information is available online at <http://npg.nature.com/reprintsandpermissions/>

**How to cite this article:** Cao, Y. *et al.* Engineered Mott ground state in  $\text{LaTiO}_{3+\delta}/\text{LaNiO}_3$  heterostructure. *Nat. Commun.* 7:10418 doi: 10.1038/ncomms10418 (2016).



This work is licensed under a Creative Commons Attribution 4.0 International License. The images or other third party material in this article are included in the article's Creative Commons license, unless indicated otherwise in the credit line; if the material is not included under the Creative Commons license, users will need to obtain permission from the license holder to reproduce the material. To view a copy of this license, visit <http://creativecommons.org/licenses/by/4.0/>